

Simulation of defects in aluminium castings using CAD models of flaws and real X-ray images

D Mery, D Hahn and N Hitschfeld

In order to evaluate the sensitivity of defect inspection systems, it is convenient to examine simulated data. This gives the possibility to tune the parameters of the inspection method and to test the performance of the system in cases where the detection is known to be difficult. In this paper, an interactive environment for the simulation of defects in radioscopic images of aluminium castings is presented. The approach simulates only the flaws and not the whole radioscopic image of the object under test. A manifold surface is used to model a flaw with complex geometry, which is projected and superimposed onto real radioscopic images of a homogeneous object according to the exponential attenuation law for X-rays. The new grey value of a pixel, where the 3D flaw is projected, depends only on four parameters: a) the grey value of the original X-ray image without flaw; b) the linear absorption coefficient of the examined material; c) the maximal thickness observable in the radioscopic image; and d) the length of the intersection of the 3D flaw with the modelled X-ray beam, that is projected into the pixel. The approach allows the user the simulation of complex flaws at any position of an aluminium casting. Simulation results of flaws like blow holes and cracks on X-ray images are shown and contrasted with real digital images with real flaws.

1. Introduction

X-ray testing is increasingly being used as a tool for NDT in industrial production. An example is the serial examination of cast light-alloy workpieces used in the car industry^[1], such as aluminium wheels and steering gears as shown in Figure 1. The material defects occurring in the casting process such as cavities, gas, inclusions, and sponging must be detected to satisfy the safety requirements; consequently, it is necessary to check 100% of the parts. Over the past decades radioscopic systems have been introduced in the automotive manufacturing industry in order to detect flaws automatically without human interaction^[2, 3, 4]. Over the years, they have not only increased quality through repeated objective inspections and improved processes, but have also increased productivity through decreased labour cost^[5]. Research and development is ongoing into automated adaptive processes to accommodate design modifications^[6, 11].

Generally, the automatic defect recognition is based on a binary classification, where a decision is performed about whether or not an initially identified hypothetical defect in an image is in fact a defect. Unfortunately, in real automatic flaw detection problems

Corresponding author: Domingo Mery is with the Departamento de Ciencia de la Computación, Pontificia Universidad Católica de Chile, Av Vicuña Mackenna 4860(143), Santiago de Chile. E-mail: dmery@ing.puc.cl

Dennis Hahn is with the Departamento de Ingeniería Informática, Universidad de Santiago de Chile (USACH), Av. Ecuador 3659, Santiago de Chile.

Nancy Hitschfeld is with the Departamento de Ciencias de la Computación, Universidad de Chile, Blanco Encalada 2120, Santiago de Chile.

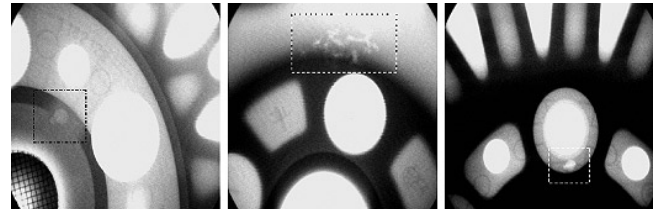


Figure 1. Real defects in radioscopic images of wheels

there are a reduced number of flaws in comparison with the large number of non-flaws. This skewed class distribution seriously limits the application of classification techniques^[7]. Usually, the performance of an inspection method can be assessed on a few images, and an evaluation on a broader and a representative database is necessary. In these cases, the evaluation on simulated data can play a significant role, because it gives the possibility of tuning the parameters of the inspection method and of testing how the method works in critical cases.

Among the NDT community there are two groups of methods to obtain this simulated data: invasive and non-invasive methods. Table 1 summarises the most important properties of them.

Invasive methods

In the invasive methods, discontinuities are produced in the test object artificially. There are two published invasive methods: i) drilling holes on the object surface^[6] (see Figure 2), and ii) designing a test piece with small spherical cavities^[8]

Table 1. Methods for simulation of defects

	Method	Description	Advantages	Disadvantages
i n v a s i v e	Drilling holes	It drills holes on the surface of the test object	<ul style="list-style-type: none"> Real X-ray image with real defects 	<ul style="list-style-type: none"> Cracks cannot be produced X-ray imaging system is required
	Spherical cavities	It produces defects inside of the test object by putting together two parts with cavities	<ul style="list-style-type: none"> Real X-ray image with real defects 	<ul style="list-style-type: none"> It destroys the test object Cracks cannot be produced X-ray imaging system is required
n o n - i n v a s i v e	Mask superimposition	It modifies the original grey value of the image by multiplying it with a factor.	<ul style="list-style-type: none"> Real X-ray image with simulated defects. Easy implementation. 	<ul style="list-style-type: none"> Simulated defects differ significantly from the real ones. X-ray imaging system is required
	Full-CAD	It simulates the X-ray imaging process by projecting a CAD model including a defect.	<ul style="list-style-type: none"> No real X-ray imaging system is required Defects and object can be modelled in 3D 	<ul style="list-style-type: none"> No real X-ray image of the test object. Sophisticated computer package Time consuming
	Flaw-CAD	It modifies the original grey value of the image by superimposing the projection of a CAD model of a flaw.	<ul style="list-style-type: none"> Real X-ray image with simulated defects Not time consuming Defects can be modelled in 3D 	<ul style="list-style-type: none"> X-ray imaging system is required

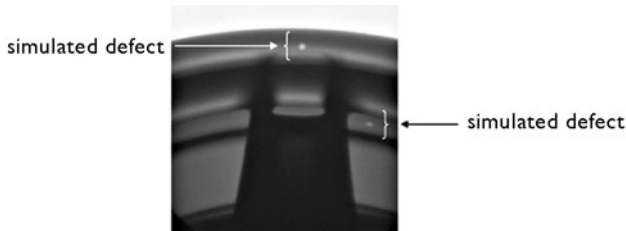


Figure 2. Two defects generated using drilling holes

(see Figure 3). Usually, the first technique drills small holes (for example $\varnothing = 1.0 \sim 4.0$ mm) in positions of the casting which are known to be difficult to detect. In the second technique, a sphere is produced for example by gluing together two aluminium pieces containing half-spherical concavities. The principal advantage of these methods is that the discontinuity image is real. However, the disadvantages are: i) it is impossible to introduce concavities in the middle of the object without destroying it, and ii) concavities like cracks are practically impossible to reproduce.



Figure 3. Two generated defects using spherical cavities^[8]

Non-invasive methods

In the non-invasive methods, X-ray images are generated or modified without altering the test object. There are three widespread approaches that produce this simulated data^[9]: i) mask superimposition, ii) CAD models for casting and flaw and iii) CAD models for flaws only. They will be described in further detail:

□ Mask superimposition

The first technique attempts to simulate flaws by superimposing circles with different grey values onto real radioscopic images^[3, 4, 10]. This approach is quite simple, because it does not need any complex 3D model of the object under test nor of the flaw. Additionally, it offers a real radioscopic image with real disturbances (with simulated flaws). Nevertheless, the flaws simulated by this method differ significantly from the real ones. The reason being that a real flaw does not look like a projection of a disc. This method can only be used in restricted cases. An example is shown in Figure 4.

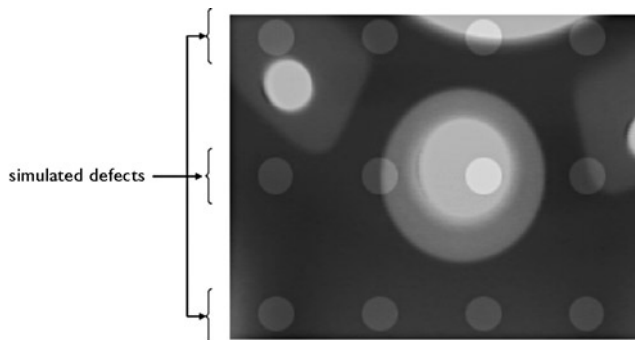


Figure 4. Simulation of twelve flaws in three rows using mask superimposition

□ CAD models for casting and flaw

The second approach makes a simulation of the entire X-ray imaging process^[11, 12, 13, 14, 15, 16]. There are many commercially available full-scale simulation tools for X-ray applications (see for example XRSIM developed at Iowa State University's Centre for Nondestructive Evaluation). In this approach, the characteristic of the X-ray source, the geometry and material properties of objects and their defects, as well as the imaging process itself are modelled and simulated independently. Complex objects and defect shapes can be simulated using

CAD models. An example is shown in Figure 5. Although this approach offers excellent flexibility in setting the objects and flaws to be tested, it presents the following three disadvantages to the evaluation of the inspection methods' performance: i) the radioscopic image of the object under test is simulated (it would be better if we could count on real images with simulated flaws); ii) the simulation approach is only available when using a sophisticated computer package; iii) it is very time-consuming.



Figure 5. Simulation of cracks using CAD models for casting and flaws (courtesy *Insight* from^[12])

□ CAD models for flaws only

In order to avoid the mentioned problems, a new approach that simulates only the flaws and not the whole X-ray image of the object under test has been presented^[17]. This method can be viewed as an improvement of the first non-invasive technique (mask superimposition) in the sense of using real digital images and of the second non-invasive technique (CAD models for casting and flaw) in the sense of allowing the user to model complex flaws. In this approach, a 3D modelled flaw is projected and superimposed onto a real X-ray image of a homogeneous object according to the exponential attenuation law for X-rays^[18]. A first approach was made in^[17], where the flaws were strictly ellipsoidal, which restricts the kind of flaws that can be superimposed. An example is shown in Figure 6.

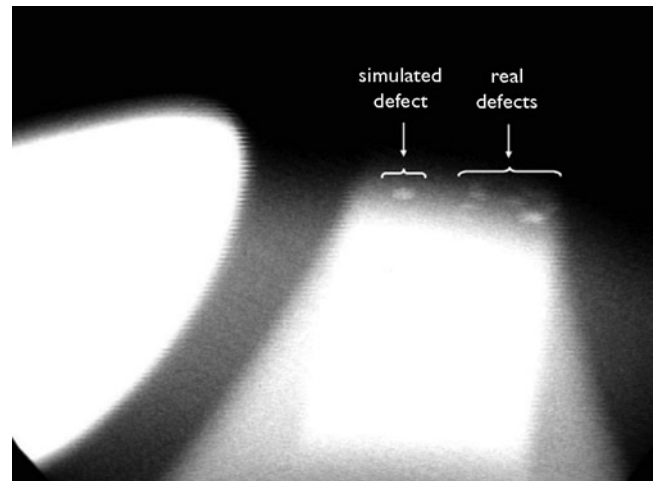


Figure 6. Simulation of a blow hole using CAD models for flaws only^[17]

In this paper, we present a general approach for the simulation of flaws on aluminium castings based on the third non-invasive technique, *ie*, using CAD models for flaws only. The flaw is modelled as an oriented manifold surface and superimposed onto real X-ray images. This approach suits best reality not only for defects like voids or blowholes, but also cracks and any complex flaw located at any position of an aluminium casting. The paper is organised as follows: In Section 2, a brief overview of the X-ray imaging process is presented. Section 3 describes how the simulation is modelled. The approach to simulate flaws in aluminium castings is outlined in Section 4. The results obtained on radioscopic images are described in Section 5. Finally, Section 6 gives concluding remarks and suggestions for future research. A first version of this research can be found in the literature^[19].

2. X-ray imaging

Radioscopic examination is a NDT technique which uses X-ray radiation to detect material defects. In this examination method,

radiation is passed through the object under test, and a detector senses the radiation intensity attenuated by the material. Thus, a defect in the material modifies the expected radiation received by the sensor^[20]. This phenomenon, called *differential absorption*, is illustrated in Figure 7, where the X-ray radiation passes through a homogeneous object containing a spherical flaw. As shown in Figure 7, the contrast in the X-ray image between an area containing a flaw and a defect-free area of the object allows distinguishing of the flaw. We can see in an X-ray image that the defects, such as voids, cracks or bubbles, show up as bright regions with respect to their neighbouring area. The reason is that the attenuation is smaller.

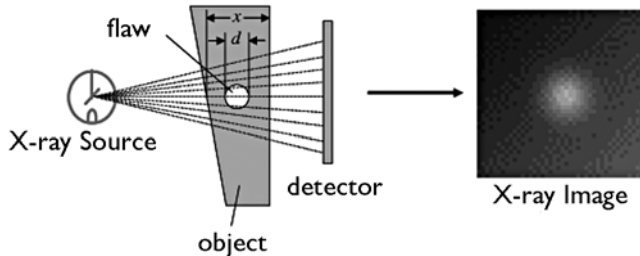


Figure 7. Differential absorption in a test object

The absorption can be macroscopically modelled using the exponential attenuation law for X-rays^[18, 20]: $\varphi(x) = \varphi_0 \exp(-\mu x)$. The incident radiation intensity φ_0 is attenuated by the object as shown in Figure 8. The transmitted intensity φ depends on the thickness of the test object x and the linear absorption coefficient μ of the object. Coefficient μ depends on the material and the X-ray energy. In Figure 8 we can observe that an X-ray beam intensity decreases exponentially with the intersection distance of the beam with the object.

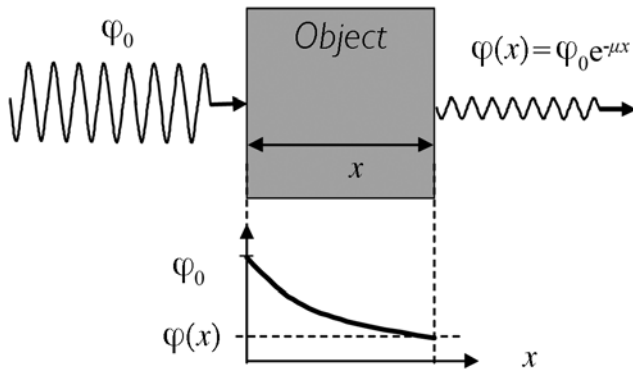


Figure 8. Attenuation law: φ_0 incident radiation intensity, φ transmitted intensity, x thickness

If we assume that the object is homogeneous, it is possible to model the grey value $I(x)$ registered by the CCD-camera as a linear function of the transmitted intensity φ : $I(x) = A\varphi(x) + B$, where A and B are the linear parameters of I . They can be estimated from the minimum and maximum grey values that the CCD-camera can register, and the maximum thickness of the object observable in the X-ray image^[17].

If the penetrated object has a cavity with thickness d as shown in Figure 7, the attenuation varies, and so does the grey value $I(x - d)$ registered by the CCD-camera. For the proposed model, these cavities are just zones of the object that have no absorption. Examples of these kinds of flaw are bubbles, cracks and voids which are very common in NDT^[21].

Using the model proposed in^[17], we can alter the original grey value of a digital X-ray image $I(x)$ to simulate a new digital image $I(x - d)$ with a flaw. The new grey value of a pixel $I(x - d)$, where the 3D flaw is projected, depends only on four parameters: a) the original grey value $I(x)$; b) the linear absorption coefficient of

the examined material μ ; c) the maximal thickness observable in the radioscopic image, and d) the length of the intersection of the 3D flaw with the modelled X-ray beam d . In this approach, the contribution of scattered radiation has not been included into the model to determine the total transmitted intensity. However, flaws can be assumed as very small perturbations that do not influence significantly the distribution of scattered radiation. Therefore, superimposing the flaw image and the radiograph from the object is an acceptable and straightforward approximation.

In the next section we describe the coordinate systems and the geometric models of each component of our simulation environment. The components are the X-ray source, the detector, the flaw and the digital image.

3. Modelling the simulation environment

The simulation considers the geometric parameters involved in the X-ray imaging system. This includes the position of the detector specified through the focal length f , the horizontal and vertical scale factors k_x and k_y , that allow us to map one pixel in the digital image with one cell in the detector, the position and behaviour of the X-ray source and the position and shape of the flaw, so that the beam hits the flaw and changes the intensity value of one pixel inside the digital image.

In the following, we describe the model of each component and the coordinate systems in which the components are specified as illustrated in Figure 9. A complete explicit model that takes into account the distortion of the X-ray imaging system introduced by the image intensifier, is given in the literature^[22].

3.1 Coordinate systems

Our simplified geometric model consists of the following two coordinate systems:

The 3D world coordinate system

This is the coordinate system of the simulation environment and allows the user to specify the position of the X-ray source, the detector and the flaw. A point in this coordinate system is denoted by M with coordinates (X, Y, Z) and the unit is measured in millimeters. The origin of this coordinate system, denoted by C in Figure 9, corresponds to the optical centre of the projection.

The 2D digital image coordinate system

The X-ray digital image is an input of the simulation process. We use a coordinate system measured in pixels. The upper left corner of the image, labelled q in Figure 9, is considered the origin of this coordinate system and a projection point is denoted by w with coordinates $(u; v)$.

3.2 Actors of the simulation

Using the coordinate systems explained in the previous section, the modelling of the four actors of the simulation will be explained.

X-ray source

The X-ray source is modelled as a plane centred in the origin C of the 3D world coordinate system as shown in Figure 9. This plane usually is lightly tilted and has small dimensions^[23]. The tilt is defined by three angles ω_x , ω_y and ω_z . During the simulation, every X-ray beam has its origin in this emitting plane and just like in a real X-ray source, the probability of a point of the plane to be an X-ray emitter is bigger when the point is near the centre of the plane. The selection of every X-ray starting point is modelled according to a double gaussian probability density function with zero mean and variances σ_x^2 and σ_y^2 given by the user.

Detector

As shown in Figure 9, the X-ray detector is modelled as a rectangle R that belongs to the $Z=f$ plane, where f corresponds to the focal length

of the X-ray projection. The detector has the same dimensions of the real detector. The idea of having this detector is to superimpose it onto the X-ray digital image, so a relation between them must be established. To achieve the superimposition, the detector has to register the same amount of values as the X-ray digital image, in other words, the detector has to be divided in enough cells to keep a one on one relation with the image pixels. The perspective projection of a 3D point (X, Y, Z) for an X-ray beam originated at point C is modelled using homogeneous coordinates as:

$$Z \begin{bmatrix} u \\ v \\ 1 \end{bmatrix} = \begin{bmatrix} -fk_u & 0 & u_0 & 0 \\ 0 & -fk_v & v_0 & 0 \\ 0 & 0 & 1 & 0 \end{bmatrix} \begin{bmatrix} X \\ Y \\ Z \\ 1 \end{bmatrix} \dots\dots\dots(1)$$

where k_u and k_v are scale factors given in pixels/mm, and u_0 and v_0 are the coordinates in the digital image of O , *ie*, the intersection of the optical axis Z with the detector plane R , as illustrated in Figure 9.

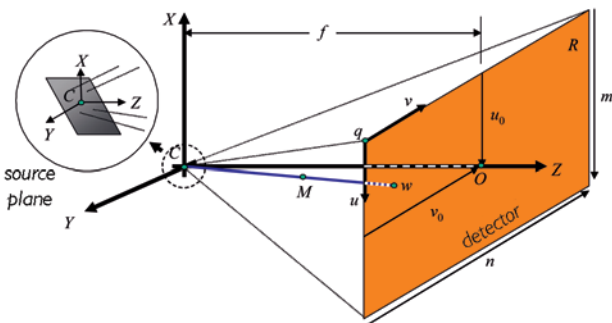


Figure 9. Projection model for the X-ray imaging

Flaw

The 3D flaw is modelled as a manifold surface in order to avoid topological singularities. This allows us to represent very well complex volumetric flaws and to concentrate our effort on algorithms that work on correct flaw shapes. Methods to correct non manifold polygonal surfaces can be found in^[24, 25]. The faces of our manifold surface are triangles.

Digital image

The X-ray digital image is represented as a matrix of $m \times n$ pixels (see Figure 9). It corresponds to the digital image coordinate system described above.

In the following section, we will explain how we produce a radioscopic image of flawed castings by simulating only the flaw.

4. Simulation of flaws

In order to simulate only the flaw and superimpose it onto an X-ray image, four steps need to be completed (see Figure 10):

- ❑ First, it is necessary to capture a real X-ray digital image taking all the needed measurements, which include focal length f , object dimensions and position, digital image scale factors k_u and k_v and digital image size (m, n) . These values are normally computed using a calibration process (see for example^[22]).
- ❑ In the second step, the 3D flaw needs to be modelled as a manifold 3D mesh. This is achieved using 3D modelling software.
- ❑ The next step consists of positioning the 3D flaw in the 3D world and of computing the length d of the part of modelled X-ray beam that pierces the 3D flaw. The length is stored in a matrix associated to the 3D world detector that is called the depth map, it is denoted by $d(u,v)$ and, just like the X-ray digital image, its dimension is $m \times n$ pixels.
- ❑ The last step consists of superimposing the depth map onto the original digital X-ray image according to the exponential attenuation law. In this step, the final X-ray digital image which contain a simulated flaw will be generated. The superimposition is performed according to Section 2.

In the following, the last two steps are described in detail, because they are the core of the simulation environment.

In order to compute the depth map, our algorithm works as follows: A single ray is emitted from every pixel of the 2D digital image coordinate system to a random point of the X-ray source plane. The distance inside the flaw is calculated and stored for each ray in a depth map cell. This process is shown in Figure 11 for the first depth map row. The intersection points between a ray and the flaw are computed and stored in a list associated to the corresponding depth map cell. This is achieved by checking the

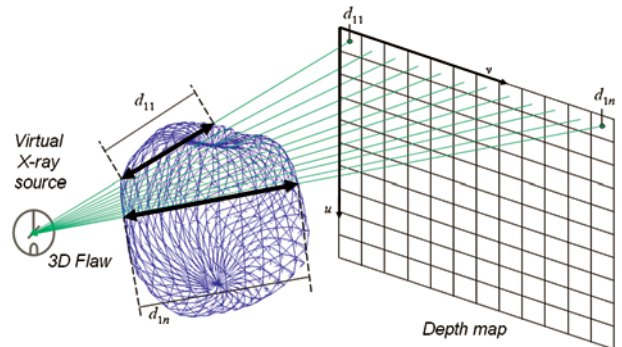


Figure 11. Depth map capture for the first row

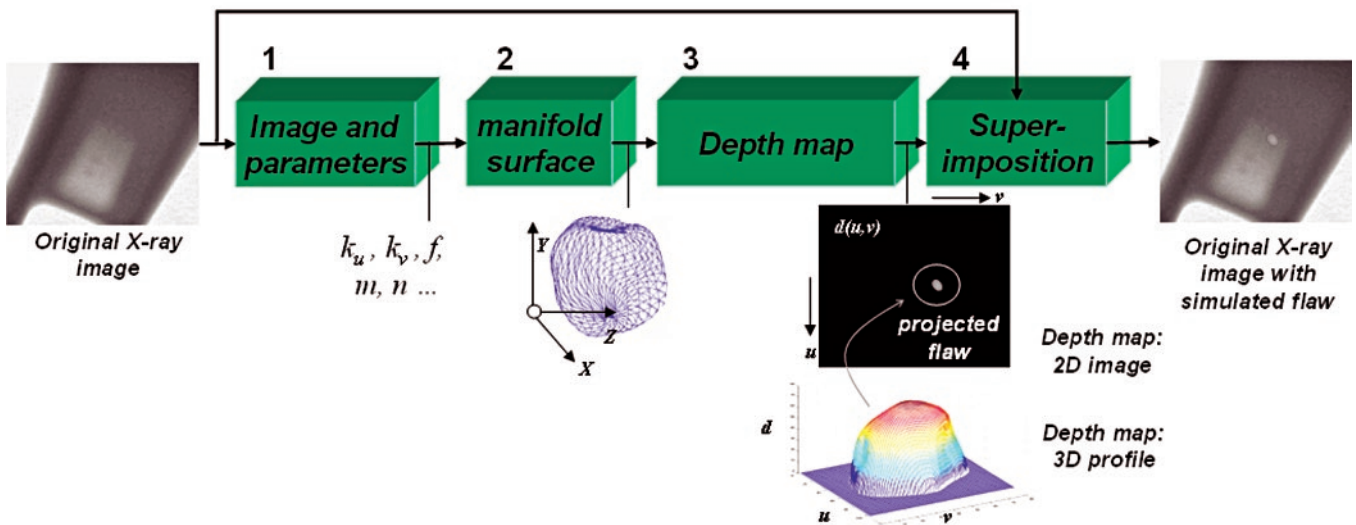


Figure 10. Flaw simulation process

intersection of a ray with each triangle in the manifold surface. The ray usually intersects an even number of triangles, because the boundary representation is assumed to be correct. However, there exist special cases, namely when the ray intersects a vertex or an edge of a triangle, where the previous statement does not hold anymore.

In order to handle the intersections between the ray and the flaw including the special cases, an algorithm based on the well-known face culling algorithm was developed^[26]. The algorithm identifies extern intersections (the ray goes into the flaw) and intern intersections (the ray goes out of the flaw), which is done by looking at the sign of the cross product vector between the ray and the normal vector of the intersected face. The special cases are handled as follows: in case the ray \mathbf{r} intersects an edge shared by face f_1 with normal vector $\hat{\mathbf{n}}_1$ and face f_2 with normal vector $\hat{\mathbf{n}}_2$, the intersection point must be only stored when the ray goes into the flaw (both faces are visible) or out of the flaws (both faces are not visible). In case $(\hat{\mathbf{n}}_1 \times \mathbf{r}) \cdot (\hat{\mathbf{n}}_2 \times \mathbf{r})$ is a negative value, the ray touches the manifold surface at that edge. A similar strategy is as follows: in order to know if a ray really enters into a flaw through a vertex or comes out of it. Once all the intersection points are stored in the list associated to each depth map cell, the portion of the ray inside the flaw is computed using Euclidean distance. Each point list is sorted using the distance between the point and the origin of the coordinate system. Since each intersection point alternates the state of the ray from outside to inside and *vice versa*, the total depth value for each ray is the sum of all the intern traces.

Figure 12 demonstrates the importance of the robustness of the collision detection method, since bogus intersections can produce defective depth maps and therefore, a non realistic simulated X-ray image. Our algorithm is very robust because it considers only real collisions and naturally eliminates bogus ones.

In order to superimpose the obtained depth map onto the input X-ray image, a simple program that calculates the new value of

each flawed image pixel was written according to the approach outlines in Section 2 (see details in the literature^[17]).

5. Experimental results

A program was developed to visualise a previously modelled 3D flaw as will as shown in Figure 13. Using this program the user can set the position, orientation and scale of manifold surface of the simulated 3D flaw.

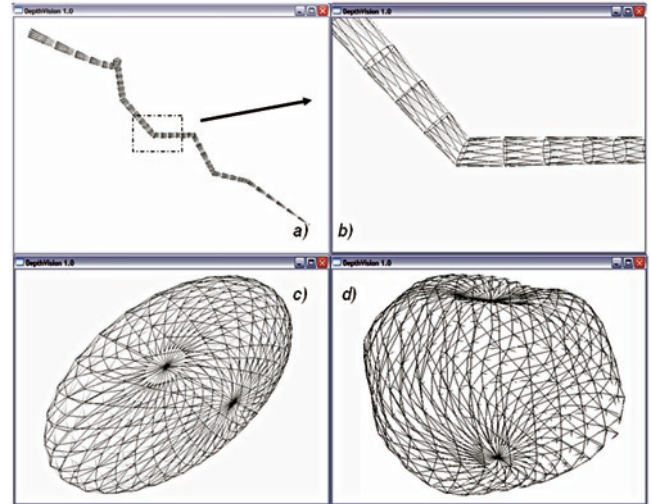


Figure 13. Manifold surfaces from the 3D modelling software: a) crack, b) zoom of a), c) ellipsoid and d) amorphous surface

The output of this program is the associated depth map and spatial correction factor files. Examples of depth maps for a blow hole and a crack are given in Figure 14 and in Figure 15 respectively, where the manifold surfaces and representations of the depth maps are shown.

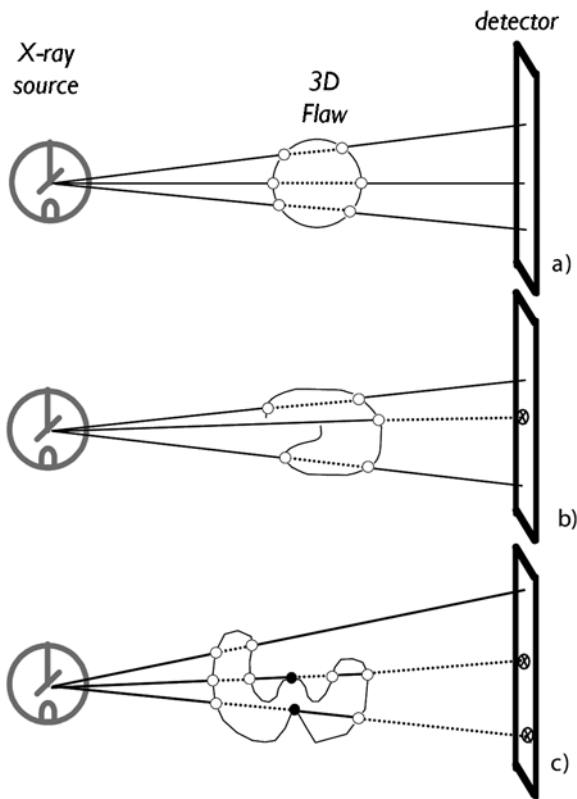


Figure 12. Calculation of a depth map. a) Closed mesh, b) error due to open mesh, c) error due to false intersections. Notation: real intersection (o); false intersection (•), wrong depth (x), X-ray outside flaw (continuous line); and X-ray inside flaw (dashed line)

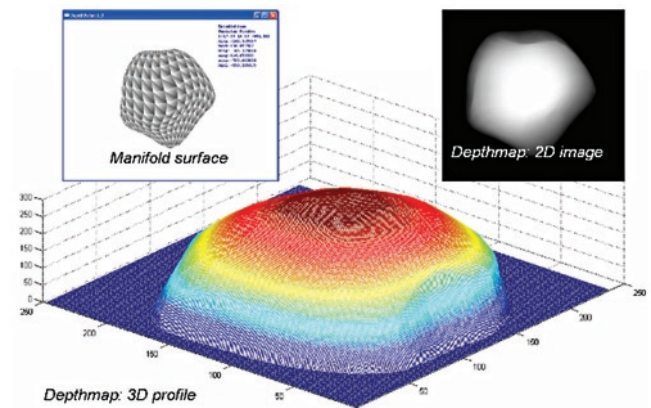


Figure 14. Depth map of a blow hole

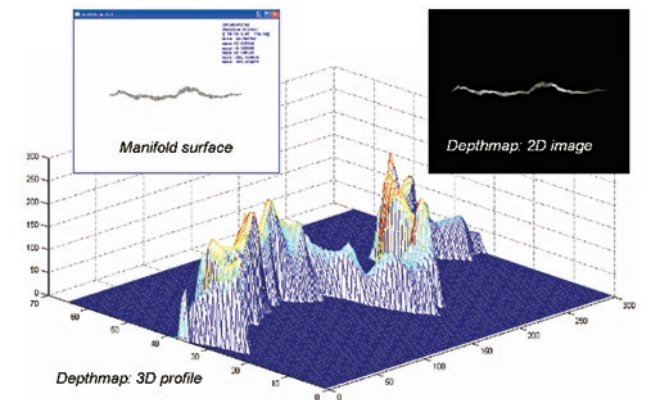


Figure 15. Depth map of a crack

Once the depth map is calculated, it can be superimposed onto a real X-ray image. A sequence is shown in Figure 16, where an ellipsoidal flaw is simulated in different positions and sizes. Each image shows a real flaw and a simulated flaw. It was shown that the simulation results are almost identical with the real flaws. Due to the irregularity of the grey values of the simulated flaw, it can be seen that both real and simulated flaws show similar patterns.

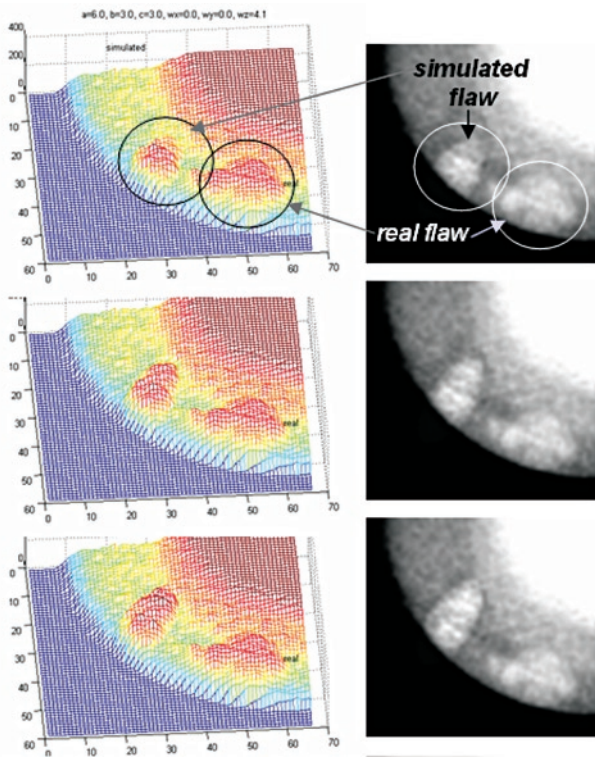


Figure 16. Sequence of different flaws: depth map and simulated image

Crack simulation can be obtained by superimposing a depth map computed from a single manifold (see, for example, Figure 15). Manifolds, depth map visualisations and the respective simulated flaw can be observed in Figure 17 for a single crack. However, a real crack corresponds to a more complex 3D representation. For this reason, we simulated another crack by superimposing several single cracks onto a real X-ray image. An example of this simulation is illustrated in Figure 18. In this case, the simulated crack is very similar to the real ones.

Simulations in this section were made on cast aluminium wheels. The dimensions of the wheels used in our experiments were 470 mm diameter and 200 mm height. The focal length was 884 mm.

6. Conclusions and future work

A new method for the simulation of defects in radioscopic images of homogeneous objects has been presented. We propose an approach that simulates the flaws using a 3D polygonal mesh model, which is projected and superimposed onto real radioscopic images. The X-ray imaging process and the projection of a 3D object have been discussed. Several simulation examples with blow holes and cracks have been illustrated. Due to the irregularity of the grey values of the simulated flaw, it can be seen that both real and simulated flaws show similar patterns.

Using this tool a simulation of a complex geometry flaw of any size and orientation can be performed in any position of the casting. This allows the precise evaluation of the performance of defect inspection systems in cases where the detection is known to be difficult.

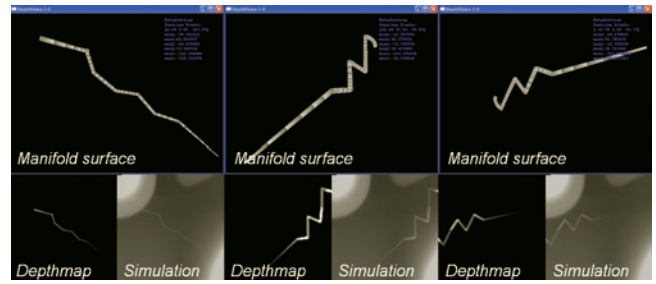


Figure 17. A manifold surface representing a crack superimposed in 3 different positions

Other open problem that we have not addressed in this paper includes the automatic generation of manifold surfaces that follows a physical flaw model. For instance, a cluster of small blow holes surfaces can simulate a porosity; and a cluster of single cracks can be used to simulate a complex crack. In order to simulate more realistic flaws, the geometric characteristics of the clusters and the single surfaces must be studied.

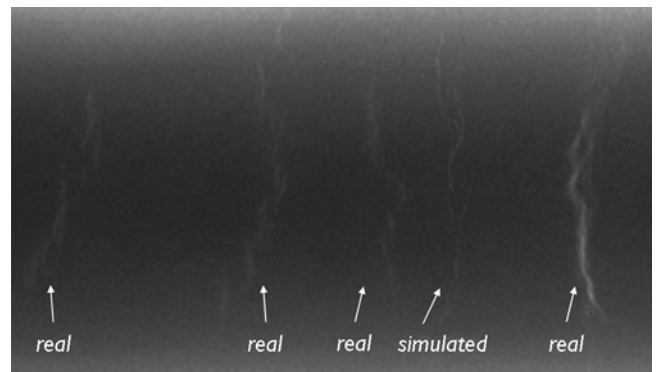


Figure 18. Simulated and real cracks

Acknowledgment

This work was supported in part by FONDECYT - Chile under grant no. 1040210.

References

1. D Mery, Th Jaeger and D Filbert, 'A review of methods for automated recognition of casting defects', *Insight*, 44(7): 428-436, 2002.
2. H Boerner and H. Strecker, 'Automated X-ray inspection of aluminium casting', *IEEE Trans. Pattern Analysis and Machine Intelligence*, 10(1):79-91, 1988.
3. D Filbert, R Klatt, W Heinrich and M Purschke. 'Computer aided inspection of castings', in *IEEE-IAS Annual Meeting*, pages 1087-1095, Atlanta, USA, 1987.
4. W Heinrich, 'Automated inspection of castings using X-ray testing', PhD thesis, Institute for Measurement and Automation, Faculty of Electrical Engineering, Technical University of Berlin, (in German), 1988.
5. F Brandt, 'The use of X-ray inspection techniques to improve quality and reduce costs', *The e-Journal of Nondestructive Testing & Ultrasonics (www.ndt.net)*, 5(5), May 2000.
6. D Mery and D Filbert, 'Automated flaw detection in aluminium castings based on the tracking of potential defects in a radioscopic image sequence', *IEEE Trans. Robotics and Automation*, 18(6):890-901, December 2002.
7. K Carvajal, M Chacón, D Mery and G Acuña, 'Neural network method for failure detection with skewed class distribution', *Insight*, 46(7):399-402, 2004.
8. K Bavendiek, 'Prüfkörper für die automatische Überprüfung der Bildqualität und der Messung der Erkennungssicherheit bei ADR Systemen'. In *German Conference on Non-destructive Testing*, Berlin, (in German), 21-23 May 2001.

9. D Mery, 'Flaw simulation in castings inspection by radioscopy', *Insight*, 43(10):664-668, 2001.
10. H Hecker, 'A new method to process X-ray images in the automated inspection of castings'. PhD thesis, Institute for Measurement and Automation, Faculty of Electrical Engineering, Technical University of Berlin, (in German), 1995.
11. G-R Tillack, C Nockemann and C Bellon, 'X-ray modelling for industrial applications', *NDT & E International*, 33(1): 481-488, 2000.
12. G-R Tillack, 'Sophisticated X-ray imaging modalities', *Insight*, 44(3):158-165, 2002.
13. N Freud, P Duvauchelle and D Babot, 'Simulation of X-ray NDT imaging techniques'. In Proceedings of the 15th World Conference on Non-Destructive Testing (WCNDT-2000), Rome, Oct. 15-21 2000.
14. P Duvauchelle, N Freud, V Kaftandjian and D Babot, 'A computer code to simulate X-ray imaging techniques', *Nuclear Instruments and Methods in Physics Research B*, 2000(170):245-258, 2000.
15. N Freud, P Duvauchelle and D Babot, 'New developments in virtual X-ray imaging: Fast simulation using a deterministic approach'. In AIP Conference Proceedings, volume 657(1), pages 553-560, 27 March 2003.
16. F Inanc and J N Grey, 'Scattering simulations in radiography', *Applied Radiation and Isotopes*, 48(10-12):1299-1305, 1997.
17. D Mery, 'A new algorithm for flaw simulation in castings by superimposing projections of 3D models onto X-ray images'. In Proceedings of the XXI International Conference of the Chilean Computer Science Society (SCCC-2001), pages 193-202, Punta Arenas, 6-8 Nov. 2001. IEEE Computer Society Press. 2001.
18. H Haken and H C Wolf, 'The Physics of Atoms and Quanta: Introduction to Experiments and Theory', Springer, Berlin, Heidelberg, 5 edition, 1996.
19. D Hahn and D Mery, 'A general approach to flaw simulation in castings by superimposing projections of 3D models onto real X-ray images'. In International Conference on Computerized Tomography for Industrial Applications and Image Processing in Radiology, German Society of Non-Destructive Testing, pages 253-264, Berlin, June 23-25 2003.
20. R Halmshaw, 'Non-Destructive-Testing'. Edward Arnold, London, 2 edition, 1991.
21. G Ogiermann and G Mann, 'Catalog of Casting Defects'. German Society of Nondestructive Testing, Oberursel, 1979.
22. D Mery, 'Explicit geometric model of a radioscopic imaging system', *NDT & E International*, 36(8):587-599, 2003.
23. D Mery, Th Jaeger and D Filbert, 'Fully automated X-ray inspection: Non-destructive testing in industrial applications', *Materialprüfung (Material Testing)*, (in German), 43(11-12):433-441, 2001.
24. F Nooruddin and G Turk, 'Simplification and repair of polygonal models using volumetric techniques', *IEEE Trans. on Visualization and Computer Graphics*, 9(2):191-205, 2003.
25. A Gueziec, G Taubin, F Lazarus and B Horn, 'Cutting and stitching: Converting sets of polygons to manifold surfaces', *IEEE Trans. on Visualization and Computer Graphics*, 7(2): 136-151, 2001.
26. J D Foley, A van Dam, S K Feiner and J F Hughes, 'Computer graphics, principles and practice'. Addison-Wesley, London, 2 edition, 1996.